J. Cent. South Univ. (2023) 30: 3322−3334
DOI: https://doi.org/10.1007/s11771-023-5371-z

Springer

Experimental study on influence of lithology on directional propagation law of type-I cracks

CHEN Le-xin(陈玏昕)[1], GUO Wei-yao(郭伟耀)[1, 2]*, JIANG Yu-jing(蒋宇静)[2], TAN Yan(谭彦)[1], ZHANG Yue-ying(张悦颖)[1], LU Dan(卢丹)[1], HAN Fei(韩飞)[3]

1. College of Energy and Mining Engineering, Shandong University of Science and Technology, Qingdao 266590, China;
2. Graduate School of Engineering, Nagasaki University, Nagasaki 852-8521, Japan;
3. Research Center for Rockburst Prevention and Control, Shandong Energy Group Co., Ltd., Jinan 250014, China

Abstract: To study the influence of lithology on the directional propagation law of rock type-I cracks, a simple crack directional propagation device was used to conduct loading tests on three rock types. The acoustic emission (AE) and displacement field characteristics during crack directional propagation were analyzed, and the propagation mechanism of type-I cracks was discussed. The results indicate that the post-peak load curve of white sandstone showed a gradually decreasing trend, while marble and grey sandstone showed a steep decreasing trend. The AE evolution during crack propagation can be divided into four stages: quiet, slowly increasing, booming, and decreasing. For white sandstone, the duration of the first three stages was short, and the decreasing stage was long. However, the opposite trend was observed for the other types. The crack propagation process includes three stages based on the evolution law of the horizontal displacement field: elastic deformation, microcrack nucleation and coalescence, and crack initiation and propagation. The white sandstone enters the microcrack nucleation and coalescence stage earlier than marble and grey sandstone. The length of the fracture process zone of white sandstone was larger than that of marble and grey sandstone; thus, its crack directional propagation rate and stability were lower.

Key words: lithology; type-I crack; digital image correlation (DIC); displacement field; acoustic emission (AE); propagation mechanism

Cite this article as: CHEN Le-xin, GUO Wei-yao, JIANG Yu-jing, TAN Yan, ZHANG Yue-ying, LU Dan, HAN Fei. Experimental study on influence of lithology on directional propagation law of type-I cracks [J]. Journal of Central South University, 2023, 30(10): 3322−3334. DOI: https://doi.org/10.1007/s11771-023-5371-z.

1 Introduction

During coal mining, a complex stress environment causes rock crack generation and rock mass cracking, expansion, and penetration. This can lead to roadway surrounding rock failure, rock bursts, and other dynamic engineering disasters [1−2]. Rock cracks are generally classified into three types according to their loading form: type-I (opening), type-II (sliding), and type-III (tearing) [3]. Type-I cracks are the primary rock failure type because the tensile strength of rock is much lower than its compressive strength [4]. Therefore, the

Foundation item: Project(52274086) supported by the National Natural Science Foundation of China; Project(ZR2019ZD13) supported by the Major Program of Shandong Provincial Natural Science Foundation, China; Project supported by Education System Government Sponsored Study Abroad Program of Shandong Province, China
Received date: 2023-04-10; **Accepted date:** 2023-06-12
Corresponding author: GUO Wei-yao, PhD, Professor; E-mail: 363216782@qq.com; ORCID: https://orcid.org/0000-0003-3589-4537

study of type-I crack propagation mechanisms is essential for understanding the rock damage process and can provide guidance for underground engineering disaster prevention and control.

Globally, researchers have conducted numerous experimental studies on the mechanisms of type-I crack propagation. The research methods used in current studies are mainly direct and indirect tensile methods [5−7]. The direct tensile method is used to obtain the tensile strength and damage characteristics by directly applying uniaxial tensile stress to a specimen. However, conducting direct tensile tests on rocks is challenging, owing to their low tensile strength. Therefore, research on the tensile mechanical properties of rocks is mainly conducted by the indirect tensile method. Brazilian disc specimens are widely used by researchers to study the mechanical properties of rock tension damage owing to their simple loading method. Through loading tests on prefabricated fissure disc specimens, researchers have investigated the effects of fissure spatial distribution [8−9] and geometric dimensions [10−12] on rock crack initiation and failure modes. However, because these studies generally used force- or displacement-controlled loading methods, controlling crack propagation was difficult, thus making it difficult to study the crack initiation and propagation process. To solve this problem, researchers have directly observed the rock damage process with the assistance of non-destructive testing methods, such as acoustic emission (AE) technique, digital image correlation (DIC), infrared camera technique, and electromagnetic radiation technique [13−16]. Among these, joint AE and DIC techniques are commonly used. The DIC technique obtains the specimen surface displacement and strain information by matching the characteristics of the speckled position changes on the specimen surface and utilizing the information to study the crack-opening displacement and fracture process zone (FPZ) length [17−19]. The AE technique obtains microcrack location and energy information with the help of time-frequency parameter processing and spatial positioning and then realizes real-time and dynamic monitoring of the crack propagation process [20−21].

Researchers have conducted studies on the evolution process of crack propagation and damage patterns in rock specimens. Although the characteristics of rock tensile damage under the influence of lithology have been studied, the law of directional crack propagation under the influence of lithology has rarely been addressed. In this study, a simple directional crack propagation test device was used to conduct experimental research on crack propagation in white sandstone, marble, and grey sandstone. The entire process of crack directional propagation was monitored using the DIC and AE techniques. The AE evolution and deformation field characteristics during the directional propagation of type-I cracks in rocks with different lithologies were investigated, and the mechanism of type-I crack propagation under the influence of lithology was explored.

2 Test method and scheme

2.1 Test method

White sandstone, marble, and grey sandstone were selected in this study. White sandstone, obtained from Zizhong County, Neijiang City, Sichuan Province, China, featured a grey-white colour, with quartz, potassium feldspar, plagioclase, and clay as the main mineral components. The marble, obtained from Longchang Mine, Neijiang City, Sichuan Province, China, featured a creamy white colour, with dolomite, calcite, and mica as the main minerals. The grey sandstone, obtained from the mining area of Chongtan Town, Naxi District, Luzhou City, Sichuan Province, China, featured a grey-black colour, with quartz, feldspar, muscovite, and siliceous material as the main mineral components. To ensure that the rock specimens had the same physical properties, each type of rock specimen was obtained from the same rock. The sampling direction was perpendicular to the rock deposition direction. According to the method recommended by the International Society of Rock Mechanics, standard specimens were prepared by coring the original rock, and uniaxial compression and Brazilian splitting tests were conducted. The physical and mechanical parameters of the rock specimens are listed in Table 1.

Table 1 Physical and mechanical parameters of rock specimen

Lithology	Density/ ($g \cdot cm^{-3}$)	Uniaxial compressive strength/MPa	Tensile strength/ MPa	Elastic modulus/ GPa
White sandstone	2.27	60.93	3.12	7.61
Marble	2.63	106.37	7.14	9.87
Grey sandstone	2.96	125.81	9.08	12.31

The rock crack directional propagation test device [22] and specimen dimensions are shown in Figure 1. The original rock obtained from the field was processed into concave specimens with dimensions of 100 mm×25 mm×100 mm. The middle of the specimen was made into a groove for fixture placement using a wire-cutting process, and a prefabricated fissure was made in the middle of the groove. The groove dimensions were 34 mm× 25 mm×35 mm, and the dimensions of the prefabricated fissure were 2 mm×25 mm×20 mm. Three specimens were tested for each type of lithology, and the most representative sets of strain fields and AE signals in each lithology were selected for analysis. In this paper, 'fissure' refers to artificial defects and cracks, ‘crack’ refers to new cracks generated during the loading process, ‘fracture’ refers to the fracture caused by crack penetration of the specimen, and ‘main control crack’ is the major type-I crack propagating along the direction of maximum stress.

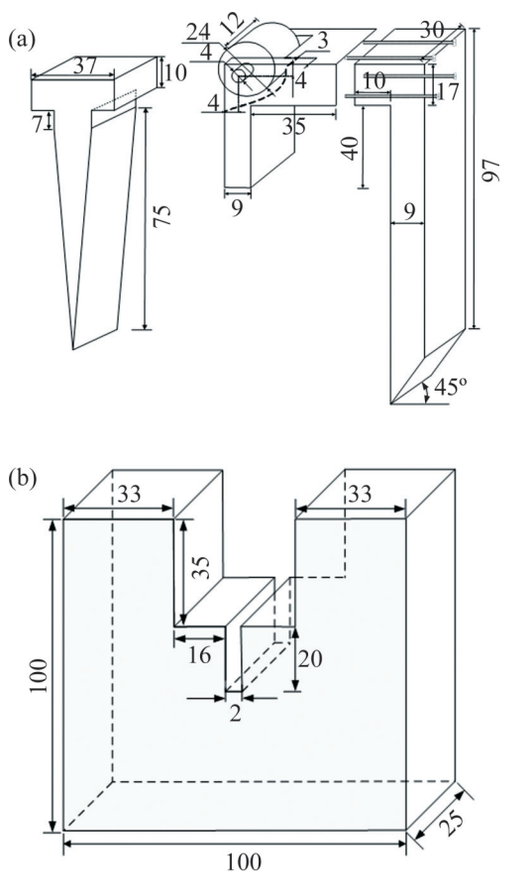

Figure 1 Rock crack directional propagation test device and specimen dimensions diagram (unit: mm): (a) Clamping device size; (b) Specimen size diagram

2.2 Test scheme

Figure 2 shows the layout of the test system. The loading system employed was a WDW-3100 universal testing machine with displacement control for uniform loading at a rate of 0.01 mm/s. AE and digital scattering monitoring systems were used for real-time observations to record the entire crack propagation process. An AMSY-6 system was used as the AE monitoring system, the preamplifier gain and threshold level were set at 38 and 40 dB, respectively, and the sampling frequency was 10 MHz. The AE probe was arranged on the rear surface of the specimen using a resin coupling agent. AE events were distributed in probe array intervals to ensure efficient acquisition of AE signals during the crack propagation process. A digital scattering system was to spray black paint on the front side of the specimen. After drying, white paint was sprayed. The sprayed white speckles were approximately 1−2 mm in size. It was ensured that the speckles were evenly and randomly distributed to enhance the image recognition acquisition effect, and the speckle displacement field of the specimen was monitored in real time throughout the loading process at a frame rate of 2 fps using a high-speed CCD camera.

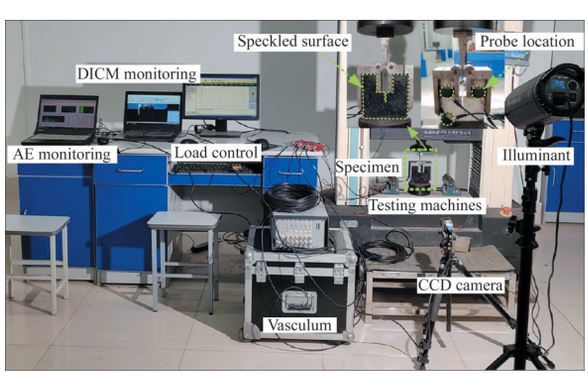

Figure 2 Test system layout

3 Analysis of test results

3.1 Load–time curve

Figure 3 shows the load – time curves for the different lithological specimens. When the upper end of the test machine was pressed downward, the tensile load on the specimen gradually increased, and the variation rate of the load curve showed a trend of initial increase and subsequent decrease. When the load reached the post-peak stage, the formation of the main control crack led to a rapid reduction in the load-bearing capacity of the specimen and a rapid decrease in the curve. The cracking processes of specimens with different lithologies differed. The post-peak curve of the white sandstone showed a gradually decreasing trend, whereas the fracture showed a graded destabilization phenomenon. In contrast, the post-peak curves of the marble and grey sandstone showed a steep decreasing trend, and the fracture exhibited an instantaneous destabilization phenomenon.

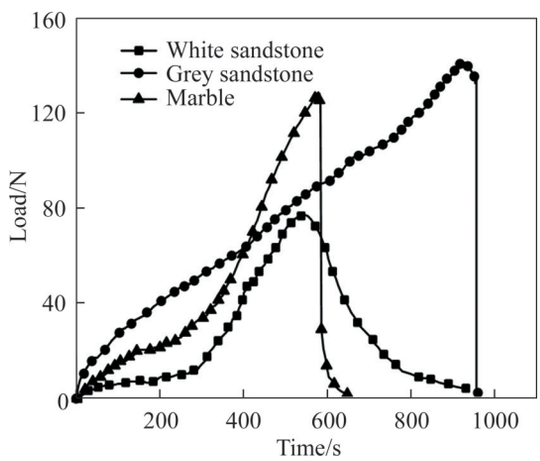

Figure 3 Load – time curves for different lithology specimens

The failure modes of the rock specimens are illustrated in Figure 4. The main control cracks for all three rock types propagated downward from the tip of the prefabricated fissure. However, some rock specimens showed a slight twist in the propagation path, likely due to the dislocation and rearrangement of local rock particles. The macroscopic fracture surfaces of the specimens were the result of crack penetration, which indirectly reflected the crack propagation paths of the specimens under tensile-stress conditions. To further explore the degree of lithological influence on crack propagation, the fracture surface of the rock specimen failure is shown in Figure 5. As shown in Figure 5(a), the fracture surface of the white sandstone was rough, with multiple grain protrusions and micropores across the fracture surface. Moreover, the fracture surface was uneven. Figures 5(b) and (c) show that the fracture surface flatness of marble and grey sandstone was higher than that of white sandstone,

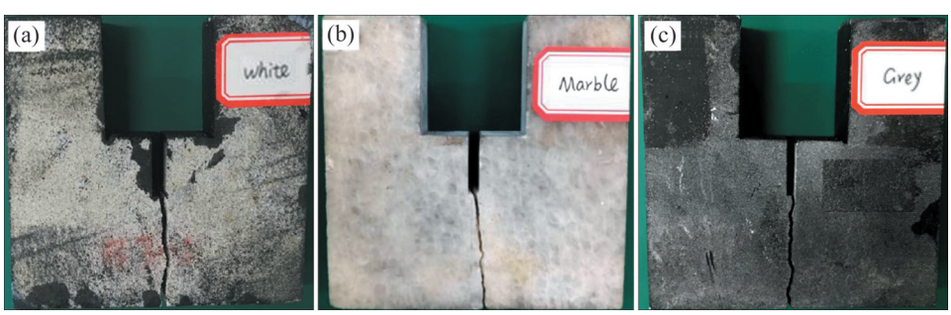

Figure 4 Failure mode of rock specimens: (a) White sandstone; (b) Marble; (c) Grey sandstone

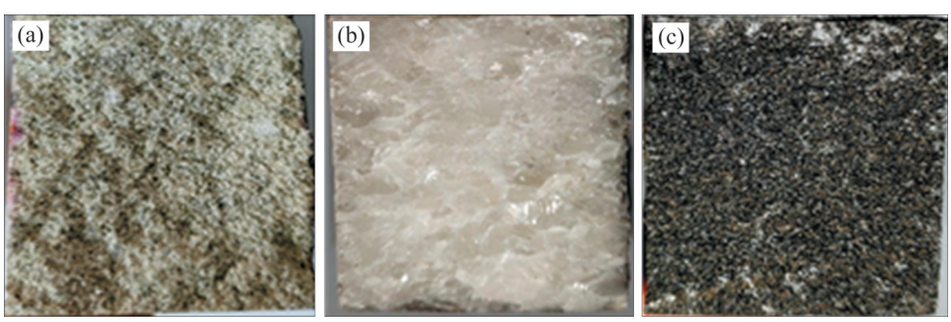

Figure 5 Fracture surface of rock specimen failure: (a) White sandstone; (b) Marble; (c) Grey sandstone

the intergranular arrangement on the fracture surface was tighter, and the fracture surface had a flat form. The flatness of the fracture surface characterized the degree of twisting in the crack propagation path. The rougher the fracture surface, the greater the degree of twisting along the crack path and the greater the instability of crack propagation. It can be observed that the stability of the main control crack propagation of white sandstone is lower than that of marble and grey sandstone. White sandstone is composed of quartz, potassium feldspar, plagioclase, and clay minerals. The presence of clay minerals may weaken the intergranular cementation strength. Primary defects and microcracks can fully develop during the loading process. Thus, the flatness of the fracture surface is lower. On the other hand, marble and grey sandstone primarily consist of high-strength mineral particles. Specifically, grey sandstone is composed of minerals such as quartz, feldspar, muscovite, and siliceous materials. They have a higher intergranular cementation strength. Microcracks can rapidly develop to form the main control cracks during the loading process, inducing higher flatness of the fracture surface and obvious brittle damage characteristics.

3.2 AE characteristics

Figure 6 shows the characteristics of the AE signals of the different lithology specimens during

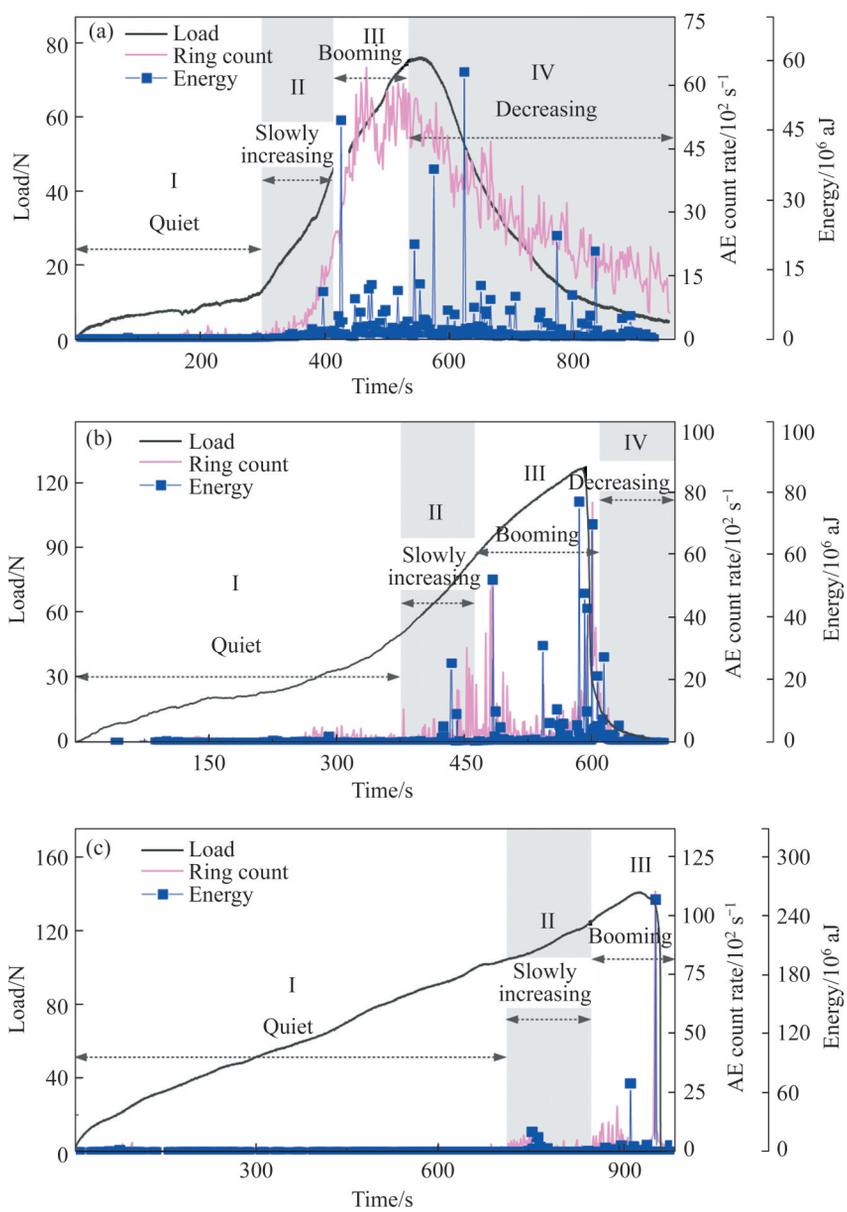

Figure 6 Characteristics of AE signals of different lithology specimens (1 aJ=10^{-18} J): (a) White sandstone; (b) Marble; (c) Grey sandstone

the fracture process. According to the characteristics of the AE signal, the crack propagation process can be divided into four stages: I, quiet period; II, slowly increasing period; III, booming period; and IV, decreasing period. During the early stage of specimen loading, the primary pores inside the specimen were in a closed state under pressure, and the AE ring count rate and energy were at low levels, indicating a quiet period. With an increase in the load, a few microcracks sprouted inside the specimen and converged into nucleation at a stable rate. The extent of crack propagation gradually increased. The AE ring count rate and energy exhibited a stable increasing trend, indicating a slowly increasing period. When approaching the peak load, the microcrack distribution density increased rapidly, and the microcrack nucleation area penetrated to form the primary control crack. The AE ring count rate increased rapidly, and the energy fluctuated more drastically than in the previous period, indicating a booming period. In the post-peak stage, the main control crack expanded and penetrated, eventually resulting in macroscopic damage. The AE ring count rate and energy continued to decay, corresponding to a decreasing period.

Distinct differences were evident in the AE evolution characteristics of the various lithology specimens. In white sandstone, during the quiet, slowly increasing, and booming periods of AE, the ringing counts and energy curves showed a rapid increase and short duration. In contrast, during the decreasing period of AE, the ringing counts and energy curves showed a gentle decrease and a more extended duration. Nevertheless, in the marble and grey sandstone, during the quiet and slowly increasing periods of AE, the ringing counts and energy curves showed a gently increasing trend with a long duration. When approaching the peak load, these curves showed a sudden increase with a short post-peak AE decreasing period. The AE evolution law reflects the differences in rock composition to a certain extent. The presence of clay in the white sandstone reduced the homogeneity of the rock and lowered its tensile strength. Therefore, the crack development in the white sandstone occurred within a short formation timeframe with slow crack propagation following the peak, indicating plastic damage characteristics. In contrast, marble and grey sandstone were cemented with siliceous material, with a uniform distribution of mineral particles and higher tensile strength. This resulted in a longer period for the development and formation of cracks in these lithology specimens. However, the cracks expanded rapidly after the peak, showing brittle damage characteristics.

3.3 DIC displacement field characteristics

The speckle calculations yielded a cloud diagram showing the evolution of the horizontal displacement field of specimens with different lithologies, as shown in Figure 7. The coloured bars on the right side of the displacement image represent the magnitude and direction of the displacement. Positive values indicate horizontal right displacement and negative values indicate horizontal left displacement. Typical states of the displacement cloud diagram during the loading process were selected for the analysis. According to the horizontal displacement field evolution law for the three rock types, the evolution process can be divided into three stages: elastic deformation (0−70%P_{max}), microcrack nucleation and coalescence (70%P_{max}− 90%P_{max}), and crack initiation and propagation (90%P_{max}−P_{max}). During the elastic deformation stage, as the load increased, the microcracks inside the specimen were compacted, and the displacement fields on the left and right sides of the prefabricated fissures were randomly distributed. The horizontal displacement difference at the fissure tip was small, i. e., there was no obvious microcrack concentration at the fissure tip at this stage. In the microcrack nucleation and coalescence stage, when the load increased to 70%P_{max}, a symmetrical partition along the centreline of the left and right specimens appeared in the lower part of the prefabricated fissure tip, and the displacement difference between the two sides of the prefabricated fissure gradually increased. This indicates that movement of the fissure tip particles occurred, and the specimen gradually approached the plastic yield from elastic deformation and entered the microcrack nucleation and coalescence stage. During the crack initiation and propagation stage, the difference in the horizontal displacement between the prefabricated fissure tips increased rapidly. The partition boundary between the left and right sides of the fissure tip gradually extended

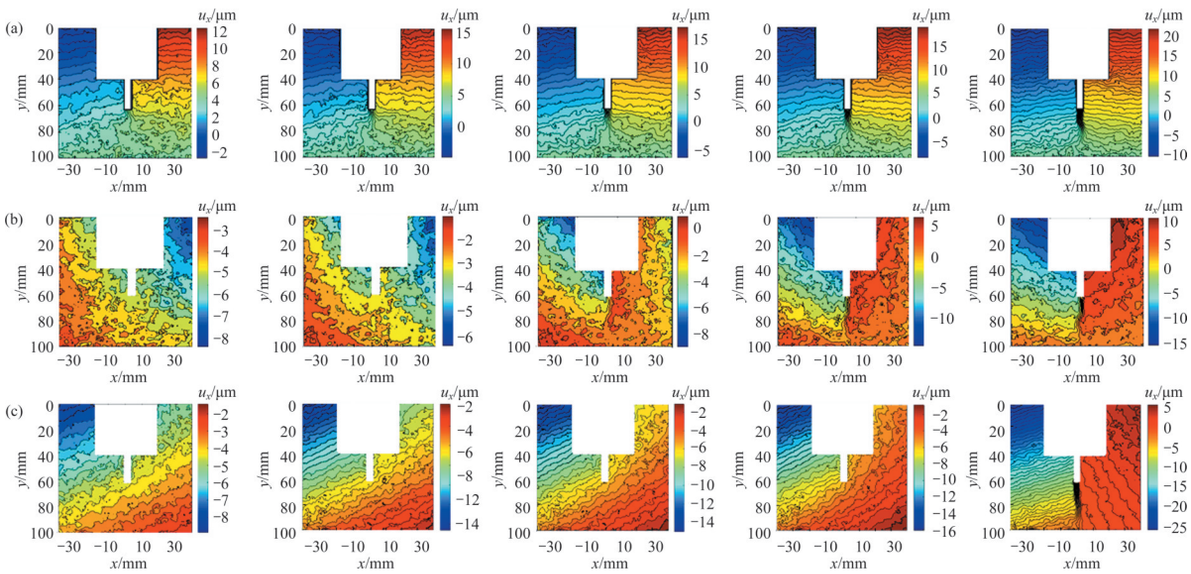

Figure 7 Cloud diagram of the horizontal displacement field evolution of different lithology specimens (unit: μm): (a) White sandstone; (b) Marble; (c) Grey sandstone

downward and formed a horizontal displacement field partition, indicating that the main control crack had begun propagating.

The evolution patterns of the horizontal displacement fields of different lithological specimens showed significant differences. As the load reached 70%P_{max}, a uniformly distributed displacement field started appearing at the fissure tip of the white sandstone, whereas the displacement fields of the marble and grey sandstone remained randomly distributed. This indicates that the microcrack nucleation time for the white sandstone was shorter than those for the marble and grey sandstone. When approaching the peak load, both sides of the centreline of the white sandstone and marble produced obvious displacement zoning, whereas the displacement field of the grey sandstone was randomly distributed. Until the peak load was reached, the nucleation zone developed into a mature state for all three lithological specimens. During the loading process, the wedge squeezed the fixture until coupling and a symmetrical condition was reached between the specimen and fixture. This process might lead to specimen deflection; in particular, the strengths of marble and grey sandstone are considerably stronger than that of white sandstone. Thus, an asymmetrical distribution of horizontal displacement in the loading range of (60% − 70%) P_{max} occurred. In summary, the speckle displacement field pattern and AE evolution characteristics during the crack propagation process showed a good agreement. The AE durations of the quiet and slowly increasing periods for white sandstone were short. The formation of displacement zoning at the fissure tip occurred early. However, the AE durations of the quiet and slowly increasing periods for marble and grey sandstone were long. Displacement zoning formed at the fissure tip only when the peak load was approached. This further indicates that lithology has a significant influence on the directional propagation mechanism of type-I cracks. This will be analyzed in detail in Section 4.

4 Influence of lithology on propagation mechanism of type-I cracks

4.1 FPZ length calculation method

The essence of type-I crack propagation is the FPZ incubation process. To investigate the characteristics of type-I crack development and evolution, researchers have proposed a cohesive zone model based on the linear elastic fracture theory [23−25], as shown in Figure 8(a). The FPZ, considered in the model as a crack with closed cohesion, formed an effective crack together with the actual crack without a cohesion constraint. When the tensile stress on both sides of the prefabricated fissure exceeded the tensile strength of the material, strain softening occurred on both sides

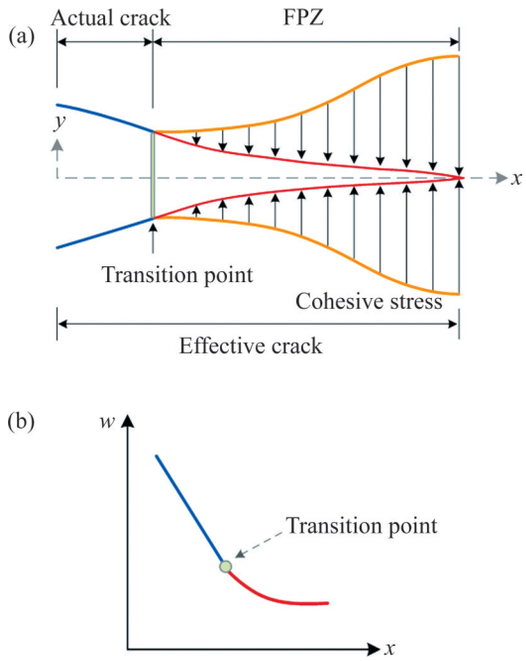

Figure 8 Schematic diagram of the cohesive zone model to identify the actual crack tip: (a) Cohesive zone model; (b) Crack-opening displacement curves

of the fissure, and the FPZ began to develop. As the load increased, the FPZ expanded along the fissure tip to the lower part, and the crack tip opening displacement gradually increased, while the cohesive force gradually decreased. At the peak load, the FPZ was fully developed. When the crack tip opening displacement reached a critical value, the crack surfaces separated from each other, and the cohesive force became 0. The effective crack length (L_e) is the sum of the actual crack length (L_a) and FPZ length (L_p). The FPZ length is a property of the material itself [25]; therefore, identifying the FPZ lengths of different lithologies is of great significance for studying the mechanism of type-I crack propagation under the influence of lithology.

The formation of an actual crack at the peak load causes the crack propagation path to change. Therefore, the accurate determination of the actual crack and effective crack tip location is a difficult task when determining the FPZ length. To identify the actual crack length L_a accurately, a coordinate system (x, y) was established at the prefabricated fissure tip, and the displacement difference at y=±16 mm boundary was defined as the crack-opening displacement w. Because there was no cohesive stress constraint between the actual cracks, the crack-opening displacement w varied linearly along the x-direction. The presence of cohesive stress in the FPZ area caused the crack-opening displacement w to vary nonlinearly along the x-direction. Therefore, the transition point between the linear and nonlinear crack-opening displacement curves was considered to be the actual crack tip [26], as shown in Figure 8(b).

According to fracture mechanics theory, displacement discontinuity is an important indicator for determining the FPZ [27−30]. The displacement value of each calculation point in the calculation area can be obtained using DIC software according to the displacement field data, and the displacement of the displacement measurement line can be extracted from it. If the horizontal displacement curve on a certain horizontal measurement line shows a continuous linear variation, the location is considered to be the FPZ tip. The effective crack length L_p is the distance from the prefabricated fissure tip to the FPZ tip. The FPZ length (L_p) was calculated using Eq. (1).

$$L_p=L_e-L_a \tag{1}$$

4.2 Crack propagation mechanism

According to Eq. (1), for the FPZ length, the difference between the effective crack length L_e and actual crack length L_a is L_p. First, the crack-opening displacement curve was used to determine the actual crack tip location. The distance from the prefabricated fissure tip (x=0) to the actual crack tip was L_a. The actual crack tips of the different lithological specimens at the peak load are shown in Figure 9. The linear and nonlinear transition points of the crack-opening displacement curves for white sandstone, marble, and grey sandstone were located at x=6.3 mm, 19.8 mm and 23.7 mm, respectively. Therefore, the L_a values of white sandstone, marble, and grey sandstone at the peak were 6.3, 19.8 and 23.7 mm, respectively.

The DIC shooting and calculation areas are shown in Figure 10. The grey area in the figure represents the calculated area. The coordinate system (u, v) was established with the prefabricated fissure tip as the coordinate origin, and a horizontal measurement line was arranged at 1 mm intervals at the prefabricated fissure tip. The u-axis shows the measured line spacing, the v-axis shows the measured line length, and the O-point is the

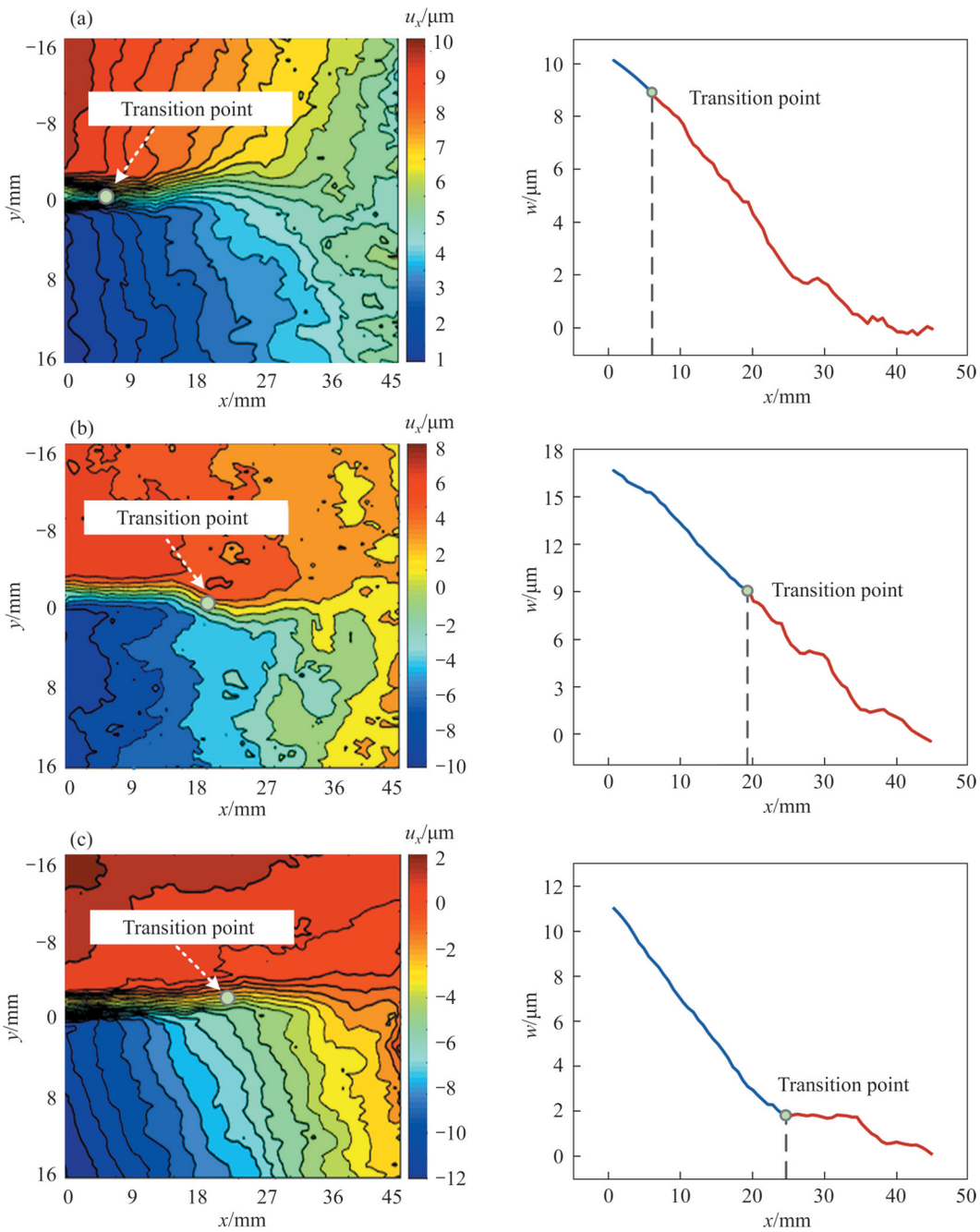

Figure 9 Actual crack tips of different lithology specimens: (a) White sandstone; (b) Marble; (c) Grey sandstone

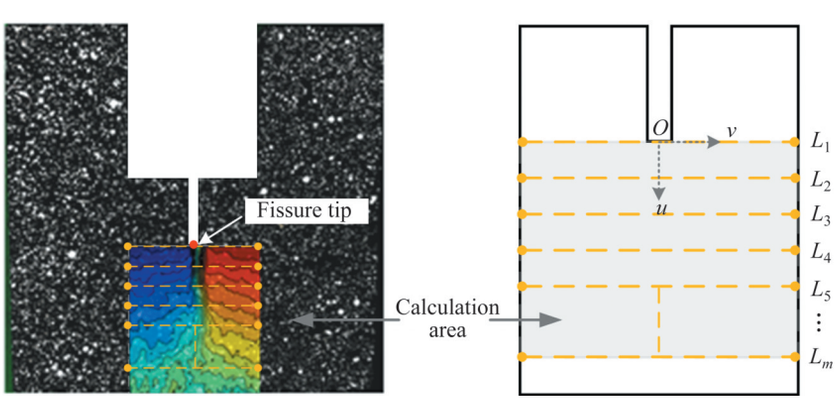

Figure 10 DIC shooting and calculation area

prefabricated fissure tip. The horizontal strain field and horizontal displacement evolution curves of the specimens with different lithologies were obtained based on the displacement data on each measurement line of the horizontal displacement field, as shown in Figure 11.

The horizontal displacement curve of white sandstone is shown in Figure 11(a). At the prefabricated fissure tip (u=0.0 mm), the horizontal displacement changes rapidly along the v-axis, showing an obvious jump fault distribution phenomenon. This jump is caused by actual fracture generation. In the range of the measurement line from u=5.0 mm to u=17.0 mm, the discontinuity of the horizontal displacement curve is obvious, but the jump of the curve keeps decreasing, and the

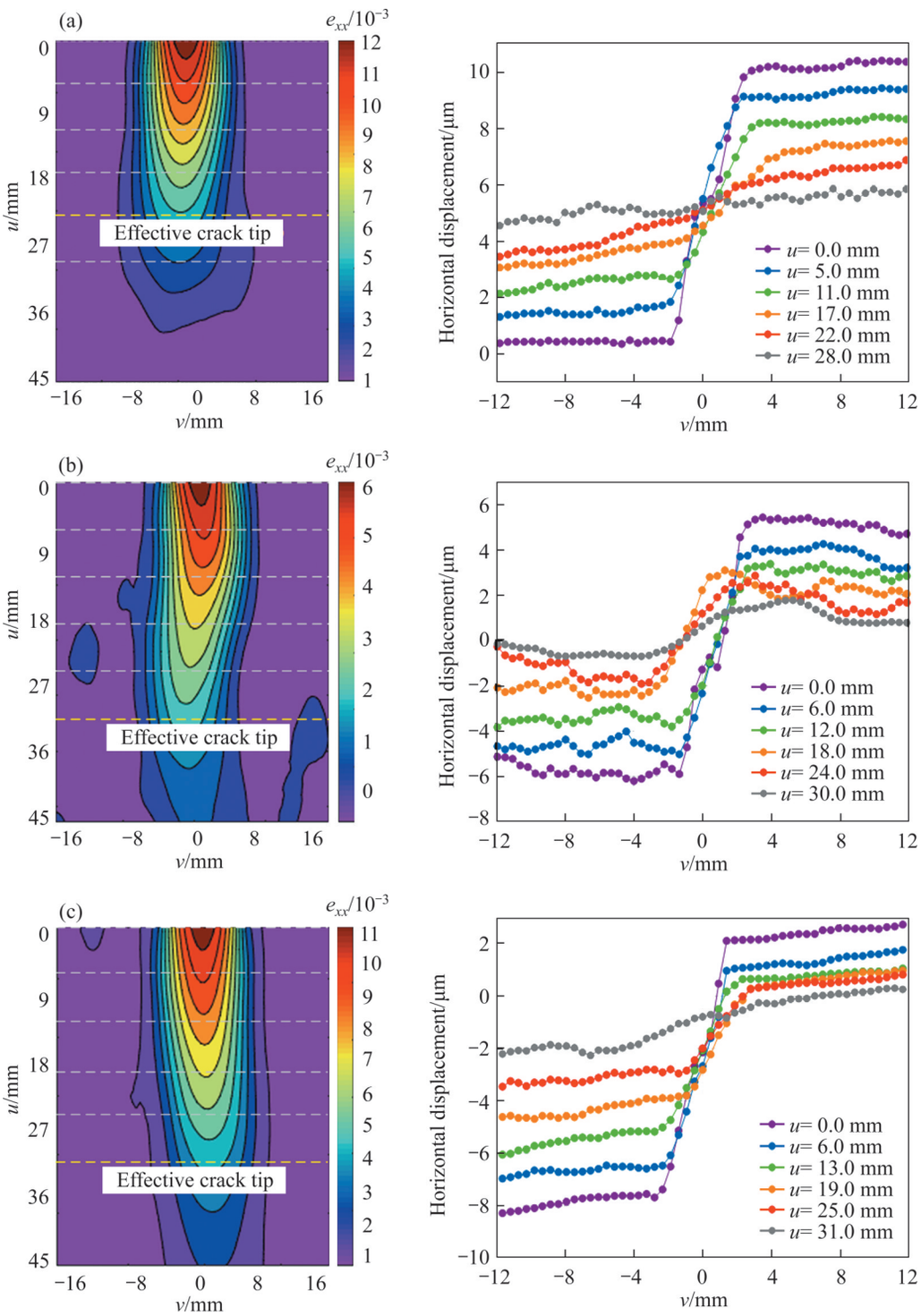

Figure 11 Horizontal strain field and horizontal displacement evolution curves of different lithology specimens: (a) White sandstone; (b) Marble; (c) Grey sandstone

degree of discontinuity change also continues to decrease, indicating that the influence of FPZ on horizontal displacement change is decreasing gradually. At u=22.0 mm, the displacement curve jumps completely disappeared, and the displacement change is continuous, indicating the end of the FPZ. Therefore, the tip of the FPZ is located at u=22.0 mm along the measurement line, i. e., the effective crack length L_e of the white sandstone is 22.0 mm. The horizontal displacement curve of the marble is shown in Figure 11(b). At the measurement line u=30.0 mm, the horizontal displacement curve is linear, i. e., L_e=30.0 mm for marble. The horizontal displacement curve of grey sandstone is shown in Figure 11(c). At the measurement line u=31.0 mm, the horizontal displacement curve is continuous, i. e., L_e=31.0 mm for grey sandstone.

The FPZ lengths reflect the differences in the crack propagation mechanisms of the different lithological specimens. According to Eq. (1), the L_p values for white sandstone, marble, and grey sandstone were 15.7, 10.2 and 7.3 mm, respectively. The FPZ length of the white sandstone was significantly larger than that of the marble and grey sandstone. The FPZ comprised softened microfractures that can withstand loads. When the main control crack expanded after the peak, the inter-FPZ cohesion affected the propagation rate of the main control crack. Combined with the experimental results mentioned earlier, the post-peak load curve of white sandstone decreased at a lower rate than at of marble and grey sandstone, and the duration of the post-AE decreasing period was longer than that of marble and grey sandstone. This indicates those the longer the FPZ, the slower the crack propagation rate. The presence of a longer FPZ leads to a higher fractional anisotropy in the microcrack connection process [27]. According to the analysis of the rock fracture surface, the flatness of the fracture surface and the degree of curvature of the crack path are lower in white sandstone than in the other two lithology specimens, i. e., the longer the FPZ, the lower the stability of the rock crack directional propagation.

5 Conclusions

1) The post-peak load curve of white sandstone showed a gradually decreasing trend; however, the other two types of rocks showed a steep decreasing trend, and their fracture surfaces have higher flatness, reflecting a brittle fracture characteristic.

2) The AE evolution during the crack propagation process can be divided into four stages: quiet, slowly increasing, booming, and decreasing. For white sandstone, the duration of the quiet, slowly increasing, and booming stages is short, and the decreasing stage is long. However, for marble and grey sandstone, the opposite trend was observed.

3) The crack propagation process includes three stages based on the evolution law of the horizontal displacement field: elastic deformation, microcrack nucleation and coalescence, and crack initiation and propagation. The white sandstone entered the microcrack nucleation and coalescence stage earlier than marble and grey sandstone.

4) The propagation of type-I cracks is the generation process of fracture process zone. The length of the fracture process zone of white sandstone was larger than that of marble and grey sandstone, and thus its crack directional propagation rate and stability were lower.

Contributors

CHEN Le-xin and GUO Wei-yao designed experiments; CHEN Le-xin carried out experiments, GUO Wei-yao and JIANG Yu-jing analyzed experimental results; TAN Yan and HAN Fei analyzed DIC data; ZHANG Yue-ying and LU Dan analyzed AE data; CHEN Le-xin and GUO Wei-yao wrote the manuscript.

Conflict of interest

CHEN Le-xin, GUO Wei-yao, JIANG Yu-jing, TAN Yan, ZHANG Yue-ying, LU Dan and HAN Fei declare that they have no conflict of interest.

References

[1] ZHAO Tong-bin, GUO Wei-yao, TAN Yun-liang, et al. Case histories of rock bursts under complicated geological conditions [J]. Bulletin of Engineering Geology and the Environment, 2018, 77(4): 1529−1545. DOI: 10.1007/s10064-017-1014-7.

[2] TIAN Jin-jin, XU Dong-jing, LIU Tian-hao. An experimental investigation of the fracturing behaviour of rock-like materials containing two V-shaped parallelogram flaws [J]. International Journal of Mining Science and Technology,

2020, 30(6): 777−783. DOI: 10.1016/j.ijmst.2020.07.002.

[3] IRWIN G R. Analysis of stresses and strains near the end of a crack traversing a plate [J]. Journal of Applied Mechanics, 1957, 24(3): 361−364. DOI: 10.1115/1.4011547.

[4] WANG Jin-tao, ZUO Jian-ping. Numerical simulation on effect of heterogeneity on mode I fracture characteristics of rock [J]. Journal of Central South University, 2020, 27(10): 3063−3077. DOI: 10.1007/s11771-020-4529-1.

[5] LI Hai-bo, LI Jian-chun, LIU Bo, et al. Direct tension test for rock material under different strain rates at quasi-static loads [J]. Rock Mechanics and Rock Engineering, 2013, 46(5): 1247−1254. DOI: 10.1007/s00603-013-0406-7.

[6] HUANG Da, ZHU Tan-tan. Experimental and numerical study on the strength and hybrid fracture of sandstone under tension-shear stress [J]. Engineering Fracture Mechanics, 2018, 200: 387 − 400. DOI: 10.1016/j.engfracmech. 2018. 08.012.

[7] LIU Zao-bao, ZHOU Hong-yuan, ZHANG Wang, et al. A new experimental method for tensile property study of quartz sandstone under confining pressure [J]. International Journal of Rock Mechanics and Mining Sciences, 2019, 123: 104091. DOI: 10.1016/j.ijrmms.2019.104091.

[8] ZHANG Wei, GUO Wei-yao, WANG Zhi-qi. Influence of lateral pressure on mechanical behavior of different rock types under biaxial compression [J]. Journal of Central South University, 2022, 29(11): 3695−3705. DOI: 10.1007/s11771-022-5196-1.

[9] HAERI H, SHAHRIAR K, MARJI M F, et al. Experimental and numerical study of crack propagation and coalescence in pre-cracked rock-like disks [J]. International Journal of Rock Mechanics and Mining Sciences, 2014, 67: 20 − 28. DOI: 10.1016/j.ijrmms.2014.01.008.

[10] ZHOU Lei, ZHU Zhe-ming, QIU Hao, et al. Study of the effect of loading rates on crack propagation velocity and rock fracture toughness using cracked tunnel specimens [J]. International Journal of Rock Mechanics and Mining Sciences, 2018, 112: 25 − 34. DOI: 10.1016/j.ijrmms. 2018. 10.011.

[11] LIANG C Y, ZHANG Q B, LI X, et al. The effect of specimen shape and strain rate on uniaxial compressive behavior of rock material [J]. Bulletin of Engineering Geology and the Environment, 2016, 75(4): 1669 − 1681. DOI: 10.1007/s10064-015-0811-0.

[12] QIU Jia-dong, LUO Lin, LI Xi-bing, et al. Numerical investigation on the tensile fracturing behavior of rock-shotcrete interface based on discrete element method [J]. International Journal of Mining Science and Technology, 2020, 30(3): 293−301. DOI: 10.1016/j.ijmst.2020.03.007.

[13] CHEN Le-xin, GUO Wei-yao, ZHANG Dong-xiao, et al. Experimental study on the influence of prefabricated fissure size on the directional propagation law of rock type-I crack [J]. International Journal of Rock Mechanics and Mining Sciences, 2022, 160: 105274. DOI: 10.1016/j. ijrmms. 2022. 105274.

[14] ZHAO Tong-bin, ZHANG Peng-fei, GUO Wei-yao, et al. Controlling roof with potential rock burst risk through different pre-crack length: Mechanism and effect research [J]. Journal of Central South University, 2022, 29(11): 3706−3719. DOI: 10.1007/s11771-022-5190-7.

[15] GUAN Jun-feng, ZHANG Yu-long, MENG Jiang-feng, et al. A simple method for determining independent fracture toughness and tensile strength of rock [J]. International Journal of Mining Science and Technology, 2022, 32(4): 707−726. DOI: 10.1016/j.ijmst.2022.05.004.

[16] ZHANG Dong-xiao, GUO Wei-yao, ZHAO Tong-bing, et al. Experimental study on directional propagation of rock type-I crack [J]. Rock and Soil Mechanics, 2022, 43(S2): 231−244. DOI: 10.16285/j.rsm.2021.2188.

[17] HU Xiao-zhi, LI Qing-bin, WU Zhi-min, et al. Modelling fracture process zone width and length for quasi-brittle fracture of rock, concrete and ceramics [J]. Engineering Fracture Mechanics, 2022, 259: 108158. DOI: 10.1016/j. engfracmech.2021.108158.

[18] LIN Qing, YUAN Hui-na, BIOLZI L, et al. Opening and mixed mode fracture processes in a quasi-brittle material via digital imaging [J]. Engineering Fracture Mechanics, 2014, 131: 176−193. DOI: 10.1016/j.engfracmech.2014.07.028.

[19] XING Hao-zhe, XIE Fang, WANG Ming-yang, et al. Experimental investigation of fracture process zone of rock in dynamic mode I fracturing and its effect on dynamic crack initiation toughness [J]. Engineering Fracture Mechanics, 2022, 275: 108828. DOI: 10.1016/j.engfracmech. 2022.10 8828.

[20] GAO Ming-zhong, XIE Jing, GAO Ya-nan, et al. Mechanical behavior of coal under different mining rates: A case study from laboratory experiments to field testing [J]. International Journal of Mining Science and Technology, 2021, 31(5): 825−841. DOI: 10.1016/j.ijmst.2021.06.007.

[21] ZHANG Yan-bo, YAO Xu-long, LIANG Peng, et al. Fracture evolution and localization effect of damage in rock based on wave velocity imaging technology [J]. Journal of Central South University, 2021, 28(9): 2752 − 2769. DOI: 10.1007/s11771-021-4806-7.

[22] GUO Wei-yao, CHEN Le-xin, YIN Li-ming, et al. Experimental study on the influence of loading rate on the directional propagation law of rock mode-I cracks [J]. Theoretical and Applied Fracture Mechanics, 2023, 125: 103873. DOI: 10.1016/j.tafmec.2023.103873.

[23] JENQ Y S, SHAH S P. A Fracture toughness criterion for concrete [J]. Engineering Fracture Mechanics, 1985, 21(5): 1055−1069. DOI: 10.1016/0013-7944(85)90009-8.

[24] BAŽANT Z P, PLANAS J. Fracture and size effect in concrete and other quasibrittle materials [M]. Routledge, 2019. DOI: 10.1201/9780203756799.

[25] HILLERBORG A, MODÉER M, PETERSSON P E. Analysis of crack formation and crack growth in concrete by means of fracture mechanics and finite elements [J]. Cement and Concrete Research, 1976, 6(6): 773−781. DOI: 10.1016/0008-8846(76)90007-7.

[26] CHEN Lei, ZHANG Guang-qing, ZOU Zhi-kun, et al. The effect of fracture growth rate on fracture process zone development in quasi-brittle rock [J]. Engineering Fracture Mechanics, 2021, 258: 108086. DOI: 10.1016/j.engfracmech. 2021.108086.

[27] KRAMAROV V, PARRIKAR P N, MOKHTARI M. Evaluation of fracture toughness of sandstone and shale using digital image correlation [J]. Rock Mechanics and Rock Engineering, 2020, 53(9): 4231 − 4250. DOI: 10.1007/

s00603-020-02171-7.
[28] ZHANG Nan, HEDAYAT A, BOLAÑOS SOSA H G, et al. Estimation of the mode I fracture toughness and evaluations on the strain behaviors of the compacted mine tailings from full-field displacement fields via digital image correlation [J]. Theoretical and Applied Fracture Mechanics, 2021, 114: 103014. DOI: 10.1016/j.tafmec.2021.103014.
[29] GARG P, PANDIT B, HEDAYAT A, et al. An integrated approach for evaluation of linear cohesive zone model's performance in fracturing of rocks [J]. Rock Mechanics and Rock Engineering, 2022, 55(5): 2917−2936. DOI: 10.1007/s00603-021-02561-5.
[30] WU Qiu-hong, XIE Cheng-long, XIE You-sheng, et al. Extending application of asymmetric semi-circular bend specimen to investigate mixed mode I/II fracture behavior of granite [J]. Journal of Central South University, 2022, 29(4): 1289−1304. DOI: 10.1007/s11771-022-4989-6.

(Edited by YANG Hua)

中文导读

岩性对I型裂纹定向扩展规律影响的试验研究

摘要：为揭示岩性对岩石I型裂纹定向扩展的影响规律，采用一种简易裂纹定向扩展装置开展白砂岩、灰砂岩和大理岩3类典型岩石加载试验，研究不同类型岩石I型裂纹定向扩展过程中变形场及声发射演化特征，探讨岩性影响下I型裂纹扩展机制。研究结果表明：白砂岩峰后荷载曲线呈平缓降低趋势，而大理岩和灰砂岩峰后曲线则呈陡降趋势，且其断面平整度高于白砂岩的，脆性断裂特征更为显著；根据水平位移场演化规律，可将岩石I型裂纹扩展过程划分为弹性变形、微裂纹集结成核和裂纹起裂扩展3个阶段，而白砂岩进入微裂纹集结成核阶段则远早于大理岩和灰砂岩；岩石I型裂纹扩展全过程中声发射演化可划分为平静期、活跃期、突增期和回落期4个阶段，其中白砂岩的平静期、活跃期及突增期持续时间短、回落期持续时间长，而大理岩和灰砂岩则与之相反；岩石I型裂纹扩展的本质是断裂过程区孕育过程，由于白砂岩断裂过程区长度大于大理岩和灰砂岩的，造成其裂纹定向扩展速度及稳定程度均低于其他两类岩石。

关键词：岩性；I型裂纹；数字图像；位移场；声发射；扩展机制